Visible Light-Driven Photocatalytic Rhodamine B Degradation Using CdS Nanorods

Authors:

Haseeb Ullah, Eva Viglašová, Michal Galamboš

Date Submitted: 2022-10-31

Keywords: CdS, rhodamine B, photocatalysis, pseudo-first order kinetics

Abstract:

In this work, highly crystalline CdS nanorods (NRs) were successfully synthesized by a facile, one-step solvothermal method. The as-prepared CdS NRs powder was characterized by XRD, FESEM, Raman, PL, XPS, BET, and UV-visible techniques to evaluate the structural, morphological, and optical properties. The photocatalytic performance of the as-synthesized CdS NRs was investigated for the photodegradation of RhB dye under visible light irradiations. It has been found that CdS NRs show maximum RhB degradation efficiency of 88.4% in 120 min. The excellent photodegradation ability of the CdS NRs can be attributed to their rod-like structure together with their large surface area and surface state. The kinetic study indicated that the photodegradation process was best described by the pseudo-first-order kinetic model. The possible mechanism for the photodegradation of RhB dye over CdS NRs was proposed in this paper.

Record Type: Published Article

Submitted To: LAPSE (Living Archive for Process Systems Engineering)

Citation (overall record, always the latest version):	LAPSE:2022.0113
Citation (this specific file, latest version):	LAPSE:2022.0113-1
Citation (this specific file, this version):	LAPSE:2022.0113-1v1

DOI of Published Version: https://doi.org/10.3390/pr9020263

processes

MDPI

Article

Visible Light-Driven Photocatalytic Rhodamine B Degradation Using CdS Nanorods

Haseeb Ullah [1,*], Eva Viglašová [2] and Michal Galamboš [2,*]

[1] Department of Chemistry, Quaid-i-Azam University, Islamabad 45320, Pakistan
[2] Department of Nuclear Chemistry, Faculty of Natural Sciences, Comenius University in Bratislava, Mlynská Dolina, Ilkovičova 6, 84215 Bratislava, Slovakia; eva.viglasova@uniba.sk
* Correspondence: chemist.ktk.06@gmail.com (H.U.); michal.galambos@uniba.sk (M.G.)

Abstract: In this work, highly crystalline CdS nanorods (NRs) were successfully synthesized by a facile, one-step solvothermal method. The as-prepared CdS NRs powder was characterized by XRD, FESEM, Raman, PL, XPS, BET, and UV-visible techniques to evaluate the structural, morphological, and optical properties. The photocatalytic performance of the as-synthesized CdS NRs was investigated for the photodegradation of RhB dye under visible light irradiations. It has been found that CdS NRs show maximum RhB degradation efficiency of 88.4% in 120 min. The excellent photodegradation ability of the CdS NRs can be attributed to their rod-like structure together with their large surface area and surface state. The kinetic study indicated that the photodegradation process was best described by the pseudo-first-order kinetic model. The possible mechanism for the photodegradation of RhB dye over CdS NRs was proposed in this paper.

Keywords: CdS; rhodamine B; photocatalysis; pseudo-first order kinetics

Citation: Ullah, H.; Viglašová, E.; Galamboš, M. Visible Light-Driven Photocatalytic Rhodamine B Degradation Using CdS Nanorods. *Processes* **2021**, *9*, 263. https://doi.org/10.3390/pr9020263

Academic Editor: Olivier Monfort
Received: 30 November 2020
Accepted: 24 January 2021
Published: 29 January 2021

1. Introduction

In recent years, the ever-increasing global population, unplanned urbanization, and rapid industrialization have caused enormous environmental pollution, becoming an increasingly serious threat to the survival of human beings [1,2]. Organic dyes are considered a major class of environmental hazards, extensively produced by some industries such as the manufacture of plastics, papers, textile, food, cosmetic, drugs, and printing industries [3–5]. Most of the dyes have xenobiotic properties and complex aromatic structures and are resistant to degradation. Inhalation of organic dyes can cause eye burns, profuse sweating, vomiting, nausea, and mental confusion [6,7]. Nowadays, around 100,000 different types of synthetic dyes are produced with a production rate of 7×10^5 tons per year, and around 15% of the dyes are released into the natural ambiance [8]. The presence of dyes in waterbodies, even in a small amount, is a very concerning problem, as it not only affects the aesthetic nature but also reduces the photosynthetic activity of aquatic plants and algae in aqueous environments [9].

Various treatment methods, e.g., advanced oxidation processes [10], ion flotation [11], ozonation [12], membrane separation [13], anaerobic and aerobic treatment [14], biological treatment [15], and adsorption [16] have been used to treat wastewater containing organic dyes. However, these methods have several limitations, such as high cost, slow kinetics, and low performance. Therefore, it is important to develop an efficient and cost-effective technique for the decontamination of wastewater containing organic dyes. Recently, semiconductor-based photocatalysis has shown great potential in the remediation of the degradation of organic dyes as it can partially mineralize macromolecular organic dyes into small molecules such as H_2O and CO_2 [17]. During the photocatalysis process under visible light irradiation, the electrons excites from the filled valence band (VB) of a semiconductor to the empty conduction band (CB), generates excited electron-hole pairs, which reacts with the oxygen and hydroxyl ions to generate active radicals that can degrade

water contaminants readily and quickly [18]. Among the known semiconductor photocatalysts, titanium oxide (TiO_2) has been extensively studied and used [19]. The traditional photocatalysts such as ZnO andTiO_2 have been extensively used due to their low-cost, reusability, stability, and availability. However, their practical application as photocatalyst has been severely restricted due to their high bandgap (TiO2 ~ 3.2 eV, ZnO ~ 3.37 eV) and ultraviolet (UV) light activity that accounts only for 4% of the total UV-visible light [20–22]. Therefore, there is an imminent need to develop an efficient, low-cost visible-light active materials to tackle environmental pollution.

Among the semiconductor photocatalysts, cadmium sulfide (CdS) is the most extensively used photocatalyst in environmental remediation and one of the most important semiconductor materials (bandgap ~ 2.4 eV), absorbs in the visible region [23,24]. However, the practical usage of CdS in photocatalysis is limited due to some serious shortcomings, including particle aggregation, photo corrosion, and a short lifetime of photo-generated carriers [25,26]. In this context, various efforts have been made to improve CdS photocatalytic activity and stability, such as morphological and structural modification, ion doping, and semiconductors hybridization, etc. It is widely known that the photocatalytic properties of the semiconductor nanomaterials significantly depend on their specific properties such as size, bandgap, morphology, spatial architectures, and especially the specific surface area [27,28]. Therefore various synthetic methods have been investigated for the synthesis of 1D to 3D CdS nanostructures photocatalysts such as hydrothermal/solvothermal method, colloidal method, template method, thermal evaporation, electrochemically induced deposition method, and laser-assisted catalytic growth process [29,30]. Among all these methods, a solvothermal method is the most promising and cost-effective technique to direct and control the nanocrystalline properties of the resultant nanomaterials such as morphology, crystal phase, luminescence, and size [31]. It has been reported that CdS nanorods (NRs) with a hexagonal crystal structure, good crystallinity, and large surface area have proved higher photocatalytic activity compared to the pure cubic phases [32]. CdS NRs with a high aspect ratio showed higher photocatalytic activity due to the restrained electrons in a specific direction that influences the electronic and optical properties of the photocatalyst [33]. Liu et al. found the improved CdS photocatalytic performance due to the increase of exposed 002 facets [34].

Herein, by taking the above consideration and discussion, the main aim of our work was established. The morphology-controlled synthesis of hexagonal phase CdS NRs with high-aspect ratio, high surface area, and exposed 002 facets was performed. The photocatalytic activity of the CdS NRs for the photodegradation of rhodamine B (RhB) was investigated using visible light irradiation. Besides, the effect of several experimental parameters, viz., the catalyst dosage and the initial RhB concentration, were also examined.

2. Materials and Methods

2.1. Chemicals

Cadmium acetate dihydrate ($Cd(CH_3COO)_2{\cdot}2H_2O$), sodium diethyldithiocarbamate tetrahydrate ($C_5H_{10}NNaS_2{\cdot}4H_2O$), diethylenetriamine ($HN(CH_2CH_2NH_2)_2$), and ethanol ($C_2H_5OH$) were purchased from Sigma-Aldrich (Islamabad, Pakistan). Rhodamine B (RhB) dye was chosen as a model for the environmental pollutant. All chemicals were of reagent grade and were used as received.

2.2. Synthesis of CdS NRs

In a typical synthesis procedure, $Cd(CH_3COO)_2{\cdot}2H_2O$ (7.379 g), $C_5H_{10}NNaS_2{\cdot}4H_2O$ (5.25 g), and diethylenetriamine (120 mL) were added to a clean Teflon-lined autoclave. The mixture was vigorously stirred for 30 min to form a homogenous dispersion. The autoclave was then sealed and heated at 180 °C for 24 h in an oven and subsequently air cooled naturally. The resulting yellow product of CdS NRs was collected after centrifugation and washed with ethanol and distilled water, followed by drying at 80 °C for 10 h.

2.3. Characterization

The crystal phase identification of the photocatalyst was performed by X-ray diffraction (XRD) analysis. The XRD measurement was done using Bruker D2 Phaser diffractometer with Cu-Kα radiation (λ = 1.5406 Å) in the 2θ range between 10–80°. The structure and morphology were examined by a field emission scanning electron microscope (FESEM-EDS, Zeiss Ultra Plus), and the photoluminescence (PL) measurement was performed on a PL lifetime spectrometer (Edinburgh Instruments). The optical property was determined by using a UV-visible spectrophotometer (Shimadzu UV-1800). The electron binding energies and surface chemical composition were determined by X-ray photoelectron spectroscopy (XPS, Thermo K alpha). The pore size and surface area of the sample were measured by Brunauer–Emmett–Teller (BET) nitrogen adsorption measurement (BET Micromeritics ASAP 2020). Raman spectrum of the sample was recorded on an inVia Renishaw spectrometer.

2.4. Photocatalytic Degradation of RhB

The photocatalytic ability of the as-synthesized CdS NRs was assessed by the photocatalytic degradation of RhB under visible light irradiation using a 300 W incandescent lamp (Philips) placed at a working distance of 30 cm above the surface of the reaction medium. For RhB degradation, 10 mg sample of the CdS NRs catalyst was added into 80 mL of a 10 mg/L RhB solution. Before light illumination, the mixture was stirred continuously in the dark for 30 min to ensure desorption-adsorption equilibrium. During the subsequent irradiations, 4-mL of suspension was drawn at regular interval of time and centrifuged to obtain a clear solution. The remaining concentration of RhB dye was measured by a UV-vis spectrophotometer.

3. Results and Discussions

3.1. Structural, Chemical, and Optical Analysis of CdS NRs

The phase purity and crystallographic structure of the as-synthesized CdS NRs catalyst were investigated by using the XRD technique. The XRD pattern of CdS NRs is shown in Figure 1a. The observed diffraction peaks at 2θ 25.06°, 26.67°, 28.40°, 36.96°, 43.92°, 48.10°, 52.23°, 54.94°, and 67.31° and were assigned to the (100), (002), (101), (102), (110), (103), (112), (004), and (210) crystal planes of the hexagonal CdS, respectively (ICCD, PDF, 00-001-0780). The sharp diffraction peaks indicate the higher crystallinity of the as-synthesized CdS photocatalyst. The XRD peak intensities of the CdS NRs differ from the bulk material. It is noted that XRD peak intensity at 26.67° corresponding to (002) facet of CdS, is much more intense with a small width than all the other peaks, indicating the orientation growth of the nanorods along the c-axis [35], in agreement with FESEM results. Moreover, the XRD pattern of the as-synthesized CdS NRs did not show any peaks except for CdS, which confirms the high purity of the catalyst. The crystalline phase, homogeneity, and surface condition of the CdS NRs was further confirmed by Raman spectroscopy, as shown in Figure 1b. The CdS shows two characteristic peaks at 300 and 603 cm^{-1} corresponded to the 1LO and 2LO vibrational modes, respectively. The sharp Raman peaks indicate the high crystallinity of the synthesized photocatalyst, which is consistent with the XRD observations.

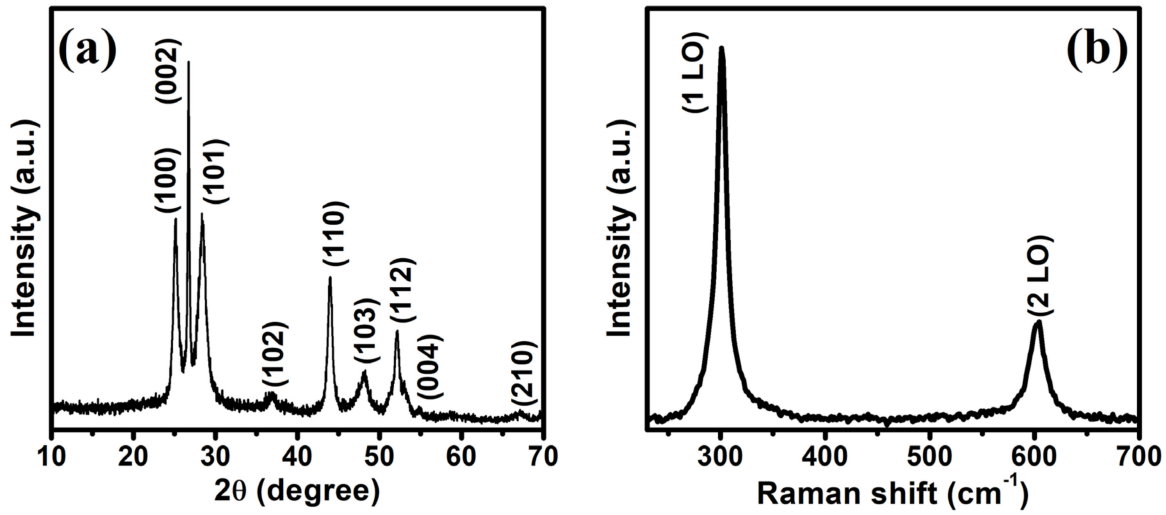

Figure 1. XRD patterns of CdS (**a**), Raman spectrum (**b**).

Field emission scanning electron microscopy (FESEM) was performed to determine the surface morphology and shape of the CdS nanostructures. The FESEM images of CdS nanostructures are shown in Figure 2, which provides clear evidence for the formation of a rod-like morphology of CdS.

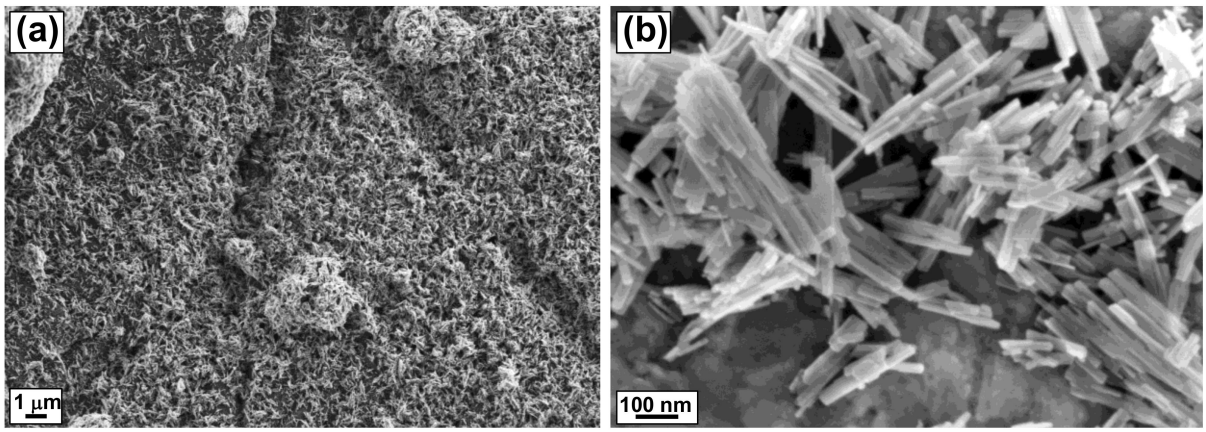

Figure 2. FESEM images of CdS NRs (**a**,**b**).

UV-visible spectrophotometric analysis (UV-vis) was performed to analyze the optical absorption properties of the as-prepared CdS NRs. Figure 3a shows the typical UV-vis spectrum of the CdS NRs in the 350–700 nm wavelength range with absorption edges at around 480 and 510 nm. The energy bandgap E_g was calculated from the following formula

$$\alpha h\nu = A\,(h\nu - E_g)^{1/2} \quad (1)$$

where α is the absorption coefficient, A is a constant, $h\nu$ is the photon energy, and E_g is the direct bandgap. The bandgap of the synthesized CdS NRs was calculated to be ~2.35 eV from the $(\alpha.E)^2$ vs. energy (eV) plot, and therefore, this nanomaterial can be used as an absorption photocatalyst over a wide range of the visible spectrum.

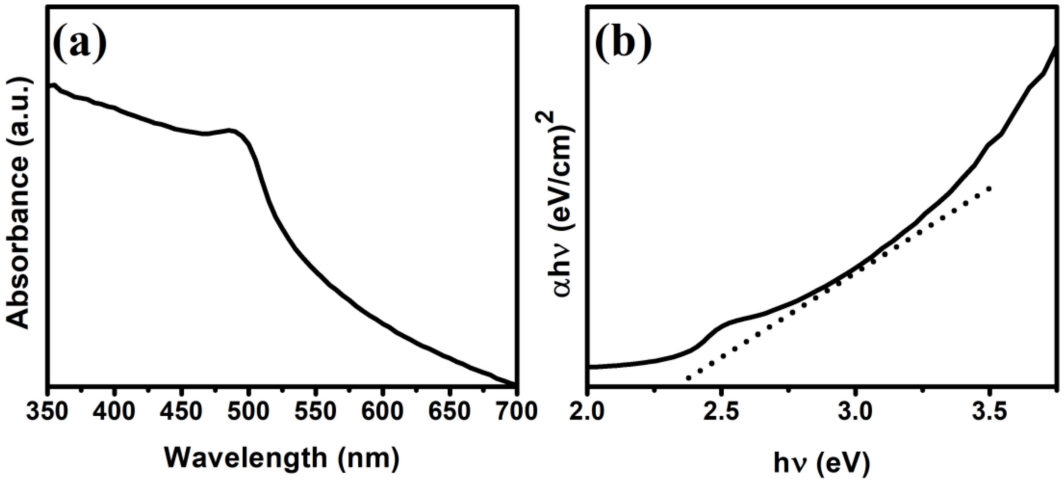

Figure 3. UV-vis DRS (**a**) and estimated bandgap energy (**b**) of CdS NRs.

The specific surface area and pore structure of CdS NRs were investigated. As shown in Figure 4, the observed isotherms can be assigned as type-IV sorption isotherms with an H3-type of hysteresis loop over a pressure range between 0.8 to 1.0 suggests the presence of slit-like pores [36]. The BET surface area of the CdS NRs was calculated as 51 m^2/g. The higher surface area of the as-synthesized CdS NRs photocatalyst compared to the reported CdS photocatalyst [37] makes the transfer of photo-generated charges easier due to the higher number of available active sites on the surface, resulting in improved photocatalytic performance. The average pore size was calculated as 32.7 nm.

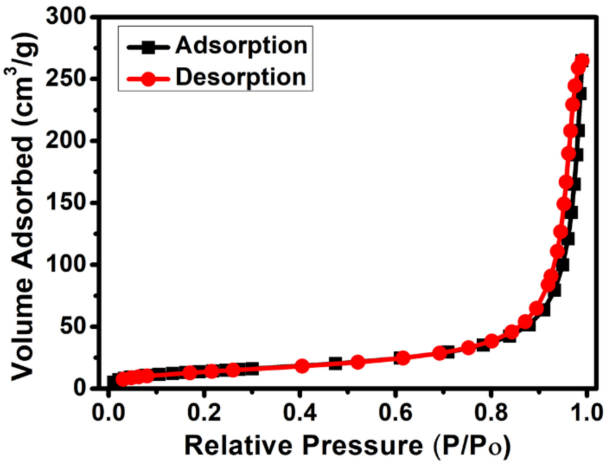

Figure 4. Nitrogen adsorption–desorption isotherm curve of CdS NRs.

The photoluminescence (PL) measurements were performed using an excitation wavelength of 380 nm to investigate the lifetime and separation of photo-induced electron-hole pairs in CdS NRs. The PL spectrum was recorded in the 425–600 nm spectral range (Figure 5a). It is well known that there is a close link between the PL data and the recombination process of photo-generated electron-hole pairs of the photocatalyst. Generally, a higher value of PL peak intensity indicates the rapid recombination of the photo-generated electron-hole pairs of the catalyst, while a lower value indicates the higher separation of photo-generated electron-hole pairs [38]. The PL emission spectrum of CdS NRs exhibits a broad emission peak around 510 nm due to the near-band-edge emission, which is consistent with the UV-vis spectroscopy results. Time-resolved PL spectrum was captured to calculate the lifetime of the photo-generated electron-hole pairs of the photocatalyst; this was found to be 1.83 ns (Figure 5b) [39].

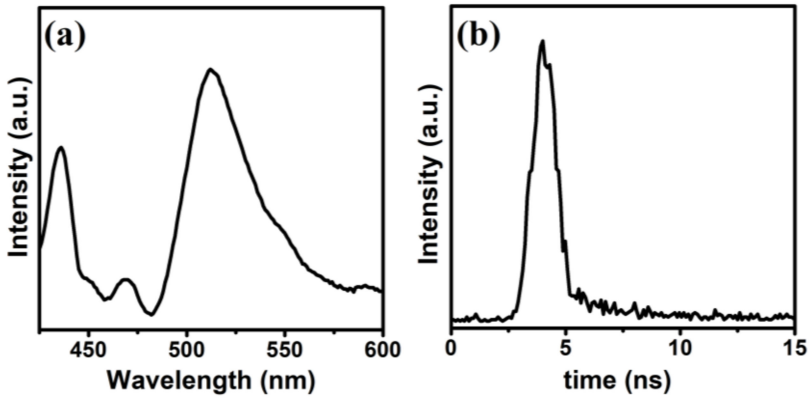

Figure 5. PL spectrum of CdS NRs (**a**), time-resolved PL spectrum (**b**).

The valence state and surface chemical composition of the CdS NRs were determined via XPS analysis. The XPS survey spectrum given in Figure 6a, show the presence of Cd and S in the majority, together with trace amount of C and O, which are probably due to contamination and adsorbed oxygen during sample exposure to the air. The two strong peaks located at 404.2 and 411.2 eV (Figure 6b) corresponds to the Cd 3d5/2 and Cd 3d3/2 states of Cd^{2+}, respectively [40]. The high-resolution S 2p spectrum in Figure 6c shows two strong peaks at 162.2 eV and 160.9 eV; and one weak peak at 168.3 eV. The strong peaks at 162.2 eV and 160.9 eV corresponds to the S 2p3/2 and S 2p1/2, respectively, which can be attributed to S^{2-} ions, while the weak peak at 168.3 eV is due to the higher valence state of S, which came from the hydrolysis of sulfur source. Figure 6d shows the binding energy of the O 1s peak of the surface adsorbed oxygen atoms on CdS.

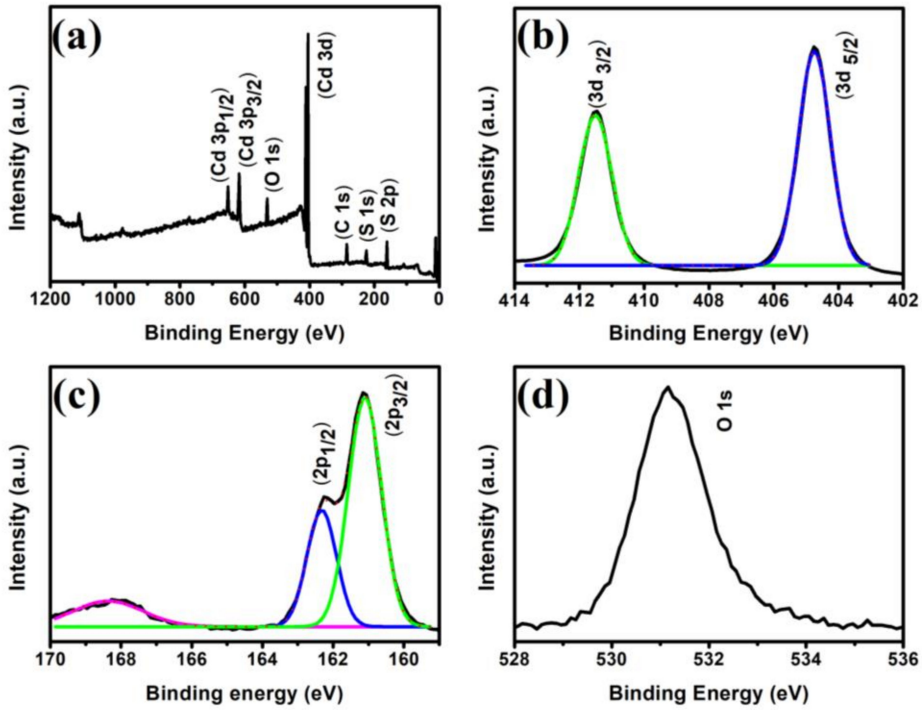

Figure 6. XPS survey spectrum of CdS NRs (**a**), high-resolution XPS spectra of Cd 3d (**b**), S 2p (**c**), and O 1s (**d**).

3.2. Photocatalytic Degradation of RhB

The photocatalytic ability of the as-prepared CdS NRs on the photodegradation of RhB in an aqueous solution under visible light illumination was investigated, and the results are shown in Figure 7. Before the photocatalytic reaction, a blank experiment without

adding photocatalyst was carried out to examine the self-degradation of RhB dye. It can be seen in Figure 7b, there is no obvious change in the concentration of dye in the absence of CdS, which suggested that the self-degradation of RhB dye during photocatalytic degradation reaction is negligible. However, by adding the photocatalyst in the solution, the absorption intensity of RhB decreases over time under visible light illumination, verifying that CdS NRs photocatalyst exhibits photocatalytic activity (Figure 7b). The photocatalytic decomposition of RhB reaches 88.4% in 120 min. However, it is very difficult to achieve the maximum degradation value during the photocatalysis process.

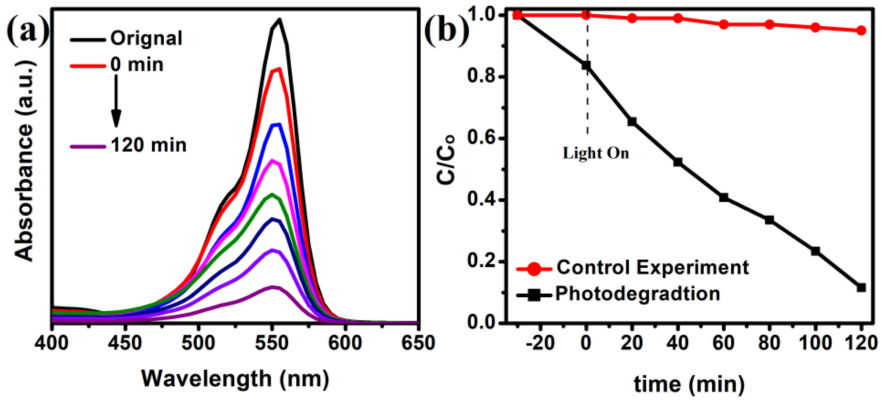

Figure 7. Time-dependent absorption spectra of RhB solution in visible light (**a**), and the degradation of RB in visible light (**b**).

The effect of photocatalyst dosage (5 mg, 7.5 mg, and 10 mg) on the photocatalytic activity was examined. As can be seen from Figure 8a, increasing the amount of CdS from 5 mg to 10 mg results in an increase in the photodegradation of RhB from 57 to 88.4%, respectively. This increase in photodegradation can be attributed to increases in the number of surface active sites and the total surface area of the catalyst available for the photocatalytic reaction [41].

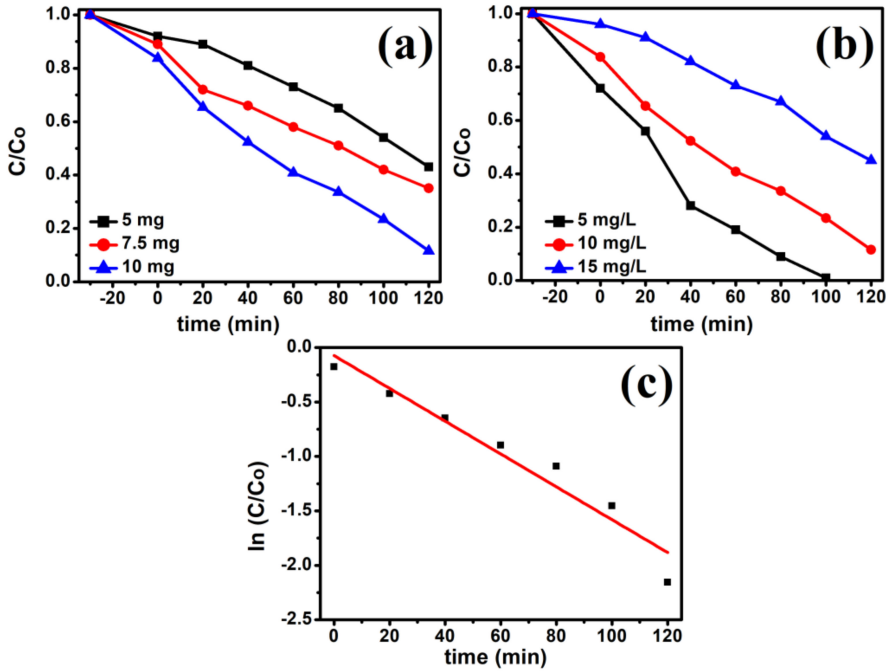

Figure 8. Effect of photocatalyst loading (**a**), Effect of initial RhB concentration (**b**), and Plot of ln (Co/C) vs. time (**c**) (10 mg photocatalyst, 10 mg/L RhB dye, Room temperature, 300 W incandescent lamp).

The effect of the initial RhB concentration on the photocatalytic activity was investigated by varying the concentration from 5 mg/L to 10 mg/L and 15 mg/L (Figure 8b), as it is an important parameter in the photodegradation of organic pollutants. The photocatalytic degradation efficiency decreases from 99 to 55% with the increase in the concentration of RhB from 5 mg/L to 15 mg/L. The reduced rate of degradation efficiency at higher concentrations is due to the unavailability of photoactive sites by increased adsorption of dye molecules and decreased rate of light penetration into the suspension [42,43]. At a high dye concentration, large portion of light is absorbed by the dye molecules, and only small portion of light is absorbed by the catalyst. As a result, the reduced photo flux reaching the catalyst surface causes a reduction in degradation efficiency.

The chemical kinetics of the photocatalytic reaction were studied to obtain some insight into the mechanism of the photodegradation process and to assess the feasibility and efficiency of treating the dye this way. The Langmuir–Hinshelwood kinetics and its pseudo-first-order reaction can be represented by the following equation as (Equations (2) and (3));

$$\frac{dC}{dt} = -K_{app}\, C \tag{2}$$

$$ln(\frac{Co}{C}) = K_{app}\, t \tag{3}$$

where K_{app} is the constant of degradation rate and t is the irradiation time. The $ln(C_o/C)$ versus t plot is shown in Figure 8c. A linear fit between $ln(C_o/C)$ and t was obtained for each plot supporting the conclusion that the photodegradation reaction follows pseudo-first-order kinetics with respect to dye concentration. The K_{app} values were calculated from the slopes of $ln(C_0/C)$ vs. t plots. For visible-light irradiation, the correlation coefficient was $R^2 = 0.945$ and the K_{app} value was 0.15×10^{-2} min^{-1}.

In addition, to study the photostability and reusability of the as-synthesized CdS NRs photocatalyst, an experiment of five consecutive cycles for the photodegradation of RhB dye was carried out. The photodegradation activity of the CdS NRs remained almost constant over five-cycles as shown in Figure 9a, suggests excellent cycling stability photocatalyst. The XRD pattern (Figure 9b) of the used photocatalyst after five cycles shows that no additional peak was observed and the crystal structure of the photocatalyst has been preserved, indicating the high stability and sustainability of the photocatalyst.

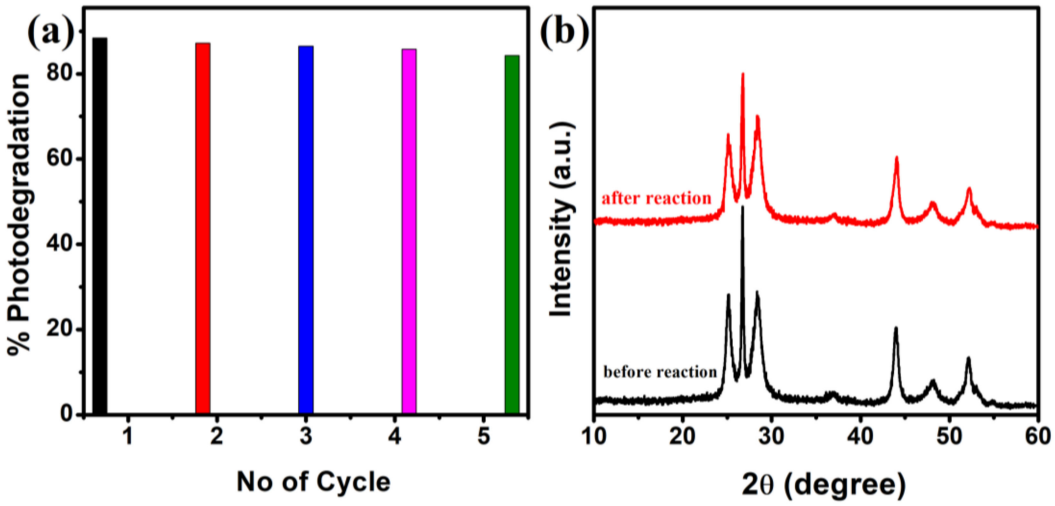

Figure 9. Stability test of CdS NRs for five cycles (**a**), XRD pattern for CdS NRs before the activity and after recycling five times for RhB photodegradation (**b**).

Figure 10, depicts the plausible mechanism for RhB dye degradation over CdS NRs. Upon visible light illumination, the electrons (ē) are excited from the filled valence band

(VB) of CdS to the conduction band (CB), creating a hole (h^+) in the VB. The generated electron from the conduction band is taken up by the adsorbed O_2 at the surface of the photocatalyst and produces superoxide radical ion ($^{\bullet}O_2^-$). The $^{\bullet}O_2^-$ further reacts with H_2O and produces hydroxyl radical ($^{\bullet}OH$) or can directly oxidize RhB dye. Simultaneously, some of the photo-induced holes (h^+) react with OH^- or H_2O to generate active specie $^{\bullet}OH$, which oxidize the adsorbed RhB dye.

$$\text{CdS NRs} + h\nu \rightarrow \text{CdS}\ (\bar{e} + h^+) \quad (4)$$

$$O_2 + \bar{e} \rightarrow O_2^- \quad (5)$$

$$O_2^- + \bar{e} + 2H^+ \rightarrow H_2O_2 \quad (6)$$

$$H_2O_2 + \bar{e} \rightarrow OH + OH^- \quad (7)$$

$$h^+ + OH^-/H_2O \rightarrow OH \quad (8)$$

$$OH + \text{RhB} \rightarrow \text{Decolourization} \quad (9)$$

$$h^+ + \text{RhB} \rightarrow \text{Decolourization} \quad (10)$$

$$O_2^- + \text{MB dye} \rightarrow \text{Decolourization} \quad (11)$$

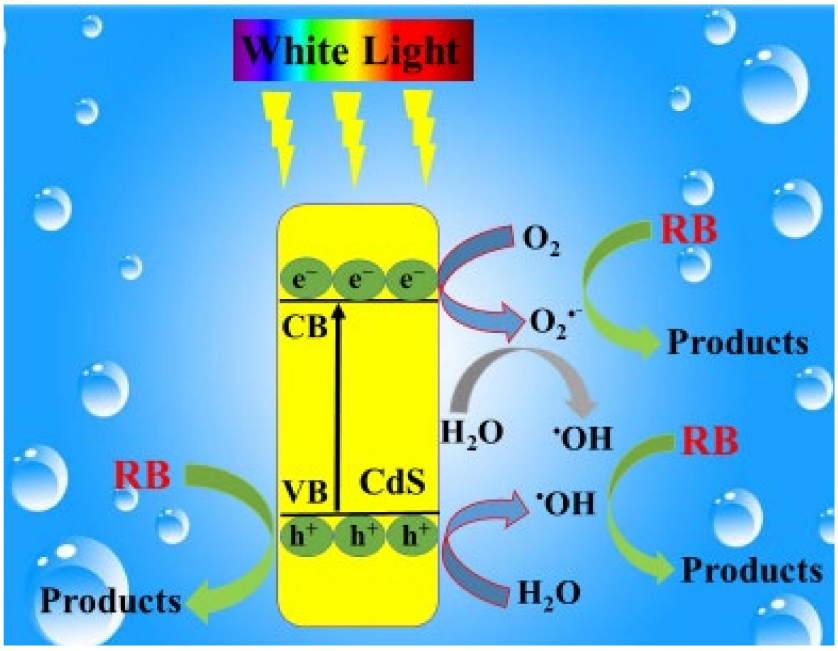

Figure 10. Proposed mechanism for the photocatalytic degradation of RB under visible light illumination.

4. Conclusions

In the present work, the highly crystalline CdS NRs were successfully synthesized by a one-step solvothermal method. The CdS NRs were characterized in terms of structure, morphological, and optical properties by XRD, Raman, FESEM, BET, PEL, UV-vis, and XPS techniques. The photocatalytic activity investigation was carried out by performing the photodegradation of RhB under visible light illumination over CdS NRs. Moreover, the photocatalytic activity of the CdS NRs depends on the various parameters such as initial dye concertation and the photocatalyst amount. It can be concluded that as-prepared CdS NRs show higher photocatalytic activity at a high dosage of photocatalyst and the low initial concentration of the RhB solution. The photodegradation of RhB follows a pseudo-first-order kinetic model.

Author Contributions: Conceptualization, H.U. and M.G.; investigation, H.U. and E.V. All authors have read and agreed to the published version of the manuscript.

Funding: This research was funded by the Higher Education Commission of Pakistan.

Institutional Review Board Statement: Not applicable.

Informed Consent Statement: Not applicable.

Data Availability Statement: The data presented in this study are available in the main text of the article.

Conflicts of Interest: The authors declare no conflict of interest.

References

1. Ferreira-Neto, E.P.; Ullah, S.; Da Silva, T.C.A.; Domeneguetti, R.R.; Perissinotto, A.P.; De Vicente, F.S.; Rodrigues-Filho, U.P.; Ribeiro, S.J. Bacterial nanocellulose/MoS2 hybrid aerogels as bifunctional adsorbent/photocatalyst membranes for in-flow water decontamination. *ACS Appl. Mater. Interfaces* **2020**, *12*, 41627–41643. [CrossRef] [PubMed]
2. Zhang, F.; Li, Y.-H.; Li, J.-Y.; Tang, Z.-R.; Xu, Y.-J. 3D graphene-based gel photocatalysts for environmental pollutants degradation. *Environ. Pollut.* **2019**, *253*, 365–376. [CrossRef] [PubMed]
3. Taghizadeh, M.T.; Siyahi, V.; Ashassi-Sorkhabi, H.; Zarrini, G. ZnO, AgCl and AgCl/ZnO nanocomposites incorporated chitosan in the form of hydrogel beads for photocatalytic degradation of MB, *E. coli* and *S. aureus*. *Int. J. Biol. Macromol.* **2020**, *147*, 1018–1028. [CrossRef] [PubMed]
4. Liu, Y.; Jin, W.; Zhao, Y.; Zhang, G.; Zhang, W. Enhanced catalytic degradation of methylene blue by α-Fe2O3/graphene oxide via heterogeneous photo-Fenton reactions. *Appl. Catal. B Environ.* **2017**, *206*, 642–652. [CrossRef]
5. Nie, L.; Zhang, Q. Recent progress in crystalline metal chalcogenides as efficient photocatalysts for organic pollutant degradation. *Inorg. Chem. Front.* **2017**, *4*, 1953–1962. [CrossRef]
6. Zhao, X.; Liu, S.; Tang, Z.; Niu, H.; Cai, Y.; Meng, W.; Wu, F.; Giesy, J.P. Synthesis of magnetic metal-organic framework (MOF) for efficient removal of organic dyes from water. *Sci. Rep.* **2015**, *5*, 11849. [CrossRef]
7. Asl, E.A.; Haghighi, M.; Talati, A. Sono-solvothermal fabrication of flowerlike Bi7O9I3-MgAl2O4 p-n nano-heterostructure photocatalyst with enhanced solar-light-driven degradation of methylene blue. *Sol. Energy* **2019**, *184*, 426–439.
8. Mahmoodi, N.M.; Abdi, J.; Oveisi, M.; Asli, M.A.; Vossoughi, M. Metal-organic framework (MIL-100 (Fe)): Synthesis, detailed photocatalytic dye degradation ability in colored textile wastewater and recycling. *Mater. Res. Bull.* **2018**, *100*, 357–366. [CrossRef]
9. Khalil, A.; Aboamera, N.M.; Nasser, W.S.; Mahmoud, W.H.; Mohamed, G.G. Photodegradation of organic dyes by PAN/SiO_2-TiO2-NH2 nanofiber membrane under visible light. *Sep. Purif. Technol.* **2019**, *224*, 509–514. [CrossRef]
10. Catalkaya, E.C.; Kargi, F. Color, TOC and AOX removals from pulp mill effluent by advanced oxidation processes: A comparative study. *J. Hazard. Mater.* **2007**, *139*, 244–253. [CrossRef]
11. Shakir, K.; Elkafrawy, A.F.; Ghoneimy, H.F.; Beheir, S.G.E.; Refaat, M. Removal of rhodamine B (a basic dye) and thoron (an acidic dye) from dilute aqueous solutions and wastewater simulants by ion flotation. *Water Res.* **2010**, *44*, 1449–1461. [CrossRef] [PubMed]
12. Zhang, J.; Lee, K.-H.; Cui, L.; Jeong, T. Degradation of methylene blue in aqueous solution by ozone-based processes. *J. Ind. Eng. Chem.* **2009**, *15*, 185–189. [CrossRef]
13. Pizzichini, M.; Russo, C.; Di Meo, C. Purification of pulp and paper wastewater, with membrane technology, for water reuse in a closed loop. *Desalination* **2005**, *178*, 351–359. [CrossRef]
14. Chan, Y.J.; Chong, M.F.; Law, C.L.; Hassell, D. A review on anaerobic–aerobic treatment of industrial and municipal wastewater. *Chem. Eng. J.* **2009**, *155*, 1–18. [CrossRef]
15. Paz, A.; Carballo, J.; Pérez, M.J.; Domínguez, J.M. Biological treatment of model dyes and textile wastewaters. *Chemosphere* **2017**, *181*, 168–177. [CrossRef]
16. Yao, X.; Ji, L.; Guo, J.; Ge, S.; Lu, W.; Cai, L.; Wang, Y.; Song, W.; Zhang, H. Magnetic activated biochar nanocomposites derived from wakame and its application in methylene blue adsorption. *Bioresour. Technol.* **2020**, *302*, 122842. [CrossRef]
17. Chen, X.; Wu, Z.; Liu, D.; Gao, Z. Preparation of ZnO Photocatalyst for the Efficient and Rapid Photocatalytic Degradation of Azo Dyes. *Nanoscale Res. Lett.* **2017**, *12*, 143. [CrossRef]
18. Li, M.; Song, C.; Wu, Y.; Wang, M.; Pan, Z.; Sun, Y.; Meng, L.; Han, S.; Xu, L.; Gan, L. Novel Z-scheme visible-light photocatalyst based on CoFe2O4/BiOBr/Graphene composites for organic dye degradation and Cr (VI) reduction. *Appl. Surf. Sci.* **2019**, *478*, 744–753. [CrossRef]
19. Romero-Saez, M.; Jaramillo, L.Y.; Saravanan, R.; Benito, N.; Pabon, E.; Mosquera, E.; Gracia Caroca, F. Notable photocatalytic activity of TiO2-polyethylene nanocomposites for visible light degradation of organic pollutants. *Express Polym. Lett.* **2017**, *11*, 899–909. [CrossRef]
20. Chen, X.; Dai, Y.; Wang, X. Methods and mechanism for improvement of photocatalytic activity and stability of Ag3PO4: A review. *J. Alloys Compd.* **2015**, *649*, 910–932. [CrossRef]

21. Li, J.; Fang, W.; Yu, C.; Zhou, W.; Zhu, L.; Xie, Y. Ag-based semiconductor photocatalysts in environmental purification. *Appl. Surf. Sci.* **2015**, *358*, 46–56. [CrossRef]
22. Hamid, S.B.A.; Teh, S.J.; Lai, C.W. Photocatalytic water oxidation on ZnO: A review. *Catalysts* **2017**, *7*, 93. [CrossRef]
23. Venkatesh, N.; Sabarish, K.; Murugadoss, G.; Thangamuthu, R.; Sakthivel, P. Visible light–driven photocatalytic dye degradation under natural sunlight using Sn-doped CdS nanoparticles. *Environ. Sci. Pollut. Res.* **2020**, *27*, 43212–43222. [CrossRef] [PubMed]
24. Nyamukamba, P.; Moloto, M.J.; Mungondori, H.H. Visible Light-Active CdS/TiO2 Hybrid Nanoparticles Immobilized on Polyacrylonitrile Membranes for the Photodegradation of Dyes in Water. *J. Nanotechnol.* **2019**, *2019*, 1–10. [CrossRef]
25. Yang, C.; Cheng, J.; Chen, Y.; Hu, Y. CdS nanoparticles immobilized on porous carbon polyhedrons derived from a metal-organic framework with enhanced visible light photocatalytic activity for antibiotic degradation. *Appl. Surf. Sci.* **2017**, *420*, 252–259. [CrossRef]
26. Hu, Y.; Gao, X.; Yu, L.; Wang, Y.; Ning, J.; Xu, S.; Ha, J.S. Carbon-Coated CdS Petalous Nanostructures with Enhanced Photostability and Photocatalytic Activity. *Angew. Chem. Int. Ed.* **2013**, *52*, 5636–5639. [CrossRef]
27. Dey, P.C.; Das, R. Enhanced photocatalytic degradation of methyl orange dye on interaction with synthesized ligand free CdS nanocrystals under visible light illumination. *Spectrochim. Acta Part A Mol. Biomol. Spectrosc.* **2020**, *231*, 118122. [CrossRef]
28. Reddy, C.V.; Vattikuti, S.P.; Shim, J. Synthesis, structural and optical properties of CdS nanoparticles with enhanced photocatalytic activities by photodegradation of organic dye molecules. *J. Mater. Sci. Mater. Electron.* **2016**, *27*, 7799–7808. [CrossRef]
29. Malik, R.; Singh, C.; Garg, R.; Kumar, V.; Singhal, S. Morphology Controlled CdS Nanostructures: A Proficient Visible-Light-Driven Photocatalyst. *Anal. Chem. Lett.* **2016**, *6*, 492–507. [CrossRef]
30. Zhang, Q.; Bu, X.; Zhang, J.; Wu, T.; Feng, P. Chiral semiconductor frameworks from cadmium sulfide clusters. *J. Am. Chem. Soc.* **2007**, *129*, 8412–8413. [CrossRef]
31. Thakur, S.; Das, P.; Mandal, S.K. Solvent-Induced Diversification of CdS Nanostructures for Photocatalytic Degradation of Methylene Blue. *ACS Appl. Nano Mater.* **2020**, *3*, 5645–5655. [CrossRef]
32. Yu, J.; Yu, Y.; Cheng, B. Enhanced visible-light photocatalytic H2-production performance of multi-armed CdS nanorods. *RSC Adv.* **2012**, *2*, 11829–11835. [CrossRef]
33. Singh, R.; Pal, B. Fine-tuning the photoluminescence and photocatalytic properties of CdS nanorods of varying dimensions. *Mater. Res. Bull.* **2013**, *48*, 1403–1410. [CrossRef]
34. Liu, Y.; Ma, Y.; Liu, W.; Shang, Y.; Zhu, A.; Tan, P.; Xiong, X.; Pan, J. Facet and morphology dependent photocatalytic hydrogen evolution with CdS nanoflowers using a novel mixed solvothermal strategy. *J. Colloid Interface Sci.* **2018**, *513*, 222–230. [CrossRef] [PubMed]
35. Ganesh, R.S.; Durgadevi, E.; Navaneethan, M.; Raji, P.; Ponnusamy, S.; Muthamizhchelvan, C.; Hayakawa, Y. Fabrication of bistable switching device using CdS nanorods embedded in PMMA (polymethylmethacrylate) nanocomposite. *J. Mater. Sci. Mater. Electron.* **2015**, *26*, 9010–9015. [CrossRef]
36. Chen, X.; Chen, W.; Lin, P.; Yang, Y.; Gao, H.; Yuan, J.; Shangguan, W. In situ photodeposition of nickel oxides on CdS for highly efficient hydrogen production via visible-light-driven photocatalysis. *Catal. Commun.* **2013**, *36*, 104–108. [CrossRef]
37. Ma, Y.; Zhao, Z.; Shen, Z.; Cai, Q.; Ji, H.; Meng, L. Hydrothermal carbonation carbon-coated CdS nanocomposite with enhanced photocatalytic activity and stability. *Catalysts* **2017**, *7*, 194. [CrossRef]
38. Rajendran, R.; Krishnakumar, V.; Jayaraman, V. Fabrication of tantalum doped CdS nanoparticles for enhanced photocatalytic degradation of organic dye under visible light exposure. *Colloids Surfaces A Physicochem. Eng. Asp.* **2019**, *580*, 123688. [CrossRef]
39. Singh, A.P.; Kumar, S.; Thirumal, M. Efficient Charge Transfer in Heterostructures of CdS/NaTaO3 with Improved Visible-Light-Driven Photocatalytic Activity. *ACS Omega* **2019**, *4*, 12175–12185. [CrossRef]
40. Cui, H.; Li, B.; Zhang, Y.; Zheng, X.; Li, X.; Li, Z.; Xu, S. Constructing Z-scheme based CoWO4/CdS photocatalysts with enhanced dye degradation and H2 generation performance. *Int. J. Hydrog. Energy* **2018**, *43*, 18242–18252. [CrossRef]
41. Devi, L.G.; Kumar, S.G. Exploring the critical dependence of adsorption of various dyes on the degradation rate using Ln3+-TiO2 surface under UV/solar light. *Appl. Surf. Sci.* **2012**, *261*, 137–146. [CrossRef]
42. Akbal, F. Photocatalytic degradation of organic dyes in the presence of titanium dioxide under UV and solar light: Effect of operational parameters. *Environ. Prog.* **2005**, *24*, 317–322. [CrossRef]
43. Salama, A.; Mohamed, A.; Aboamera, N.M.; Osman, T.A.; Khattab, A. Photocatalytic degradation of organic dyes using composite nanofibers under UV irradiation. *Appl. Nanosci.* **2018**, *8*, 155–161. [CrossRef]